

Equilibrium shape of titanium silicide nanocrystals on Si(111)

I. Goldfarb,^{1,2,*} G. Cohen-Taguri,¹ S. Grossman,¹ and M. Levinshtein¹

¹*Department of Solid Mechanics, Materials and Systems, School of Mechanical Engineering, Faculty of Engineering, Tel Aviv University, Ramat Aviv 69978, Tel Aviv, Israel*

²*University Research Institute for Nanoscience and Nanotechnology, Tel Aviv University, Ramat Aviv 69978, Tel Aviv, Israel*

(Received 15 February 2005; revised manuscript received 19 April 2005; published 18 August 2005)

The aim of this work was to find the equilibrium shape of titanium silicide nanocrystals, epitaxially grown on Si(111) in ultrahigh vacuum. To attain the state of equilibrium, the so-grown nanocrystals were subjected to a series of prolonged high-temperature annealing treatments, and closely monitored by scanning tunneling microscopy at every annealing stage. It was established, that the equilibrium shape of the equilibrium phase (C54-TiSi₂) nanocrystals grown by solid-phase epitaxy is a flat, hexagonal island with (01 $\bar{3}$) atomic plain parallel to Si(111), achieved after 750 °C anneal. The nanocrystal behavior is well described by generalized Wulf-Kaisew theorem (adjusted for epitaxial nanocrystals), with their vertical aspect ratio decreasing and the top facet area increasing upon introduction of misfit dislocations at the nanocrystal-substrate interface. Screw dislocations were also observed, and seemed to play a role in facilitating the three-dimensional-to-two-dimensional shape transformation.

DOI: [10.1103/PhysRevB.72.075430](https://doi.org/10.1103/PhysRevB.72.075430)

PACS number(s): 61.46.+w, 81.15.Kk, 64.70.Rh, 68.37.Ef

I. INTRODUCTION

Thin titanium silicide films have been commonly used in microelectronics as a contact material due to its low electrical resistivity and high contact stability.¹ Epitaxial layers could serve this purpose even better, however, growth of such high-quality titanium silicide epilayers on silicon substrates is impeded by a large lattice and symmetry mismatch between the two materials. In addition, the formation of the thermodynamically stable C54-TiSi₂ phase in thin layers is kinetically delayed by a low-temperature metastable C49-TiSi₂ with inferior properties.² However, discontinuous layers of silicides of cobalt and titanium, in the form of nanoislands,³⁻⁷ have recently drawn attention to these materials from a totally different perspective, namely as quantum-dot materials.⁵ Indeed, single electron tunneling in TiSi₂ nanoislands has been observed by Oh and co-workers even at room temperature.⁸ However, unique nanoscale properties of such self-assembled islands are a sensitive function of their size and shape which, in turn, largely depend on the competition between the relaxation and surface+interface energy terms, and are expected to be different for the two TiSi₂ polymorphs: C49 is base-centered orthorhombic containing 4 Ti and 8 Si atoms in a unit cell and can be regarded as a layered structure with an ABABA...stacking, whereas C54 is face-centered orthorhombic, with 8 Ti and 16 Si atoms in the unit cell and is stacked in a ABCDA...sequence.⁵ Hence, the nanocrystal ability or inability to evolve with temperature and time is of the utmost importance, as well as its energetic state relative to thermodynamic (or some local) equilibrium. Establishing these parameters was the aim of the present work.

II. EXPERIMENTAL

n-type Si(111) wafers were chemically degreased and introduced into an ultrahigh vacuum (UHV) variable-

temperature scanning probe microscopy (VT-SPM) system (Omicron GmbH). In addition to the SPM scanner, the system is equipped with low- (LEED) and reflection high- (RHEED) energy electron diffraction apparatus, where LEED's four-grid analyzer can also be operated in Auger electron spectroscopy (AES) mode. For epitaxial growth experiments, the system is equipped with a precise electron-beam evaporator directed at the SPM stage, so that continuous substrate scanning can be conducted during the evaporation. About 2 monolayers of titanium were evaporated onto the substrate at room temperature (RT), and subsequently annealed at various temperatures. (Since metastable C49-TiSi₂ polymorph is surface-stabilized, it can be expected to form in such a thin layer.) All the images shown in this work were acquired in the scanning tunneling microscopy (STM) mode, using conventional bias and current settings.

III. RESULTS

Three-dimensional (3D) view of titanium silicide nanocrystals as a function of temperature, after RT deposition, is shown in Fig. 1, where Fig. 1(a) is the Ti/Si(111) surface annealed at 560 °C, Fig. 1(b) is the same surface annealed at 600 °C, and Fig. 1(c) is after the 660 °C anneal. It is obvious, that with the progress of anneal, the mean size of 3D silicide nanoisland increases, the number density decreases, and the islands develop top facet, that is getting bigger and bigger. While some of the islands are two-dimensional (2D), in the shape of flat triangles and hexagons, the majority is small 3D "lenses" and "cones," which become progressively truncated. The side facets are evolving as well, when going from Figs. 1(a)–1(c). Hence, "cones" turn into flat-topped multifaceted "domes." Some of these "domes" grow even bigger, forming large "superdomes," as shown in Fig. 2(b), upon annealing at temperatures between 700 °C and 750 °C. They are so big, that only large areas, 500 × 500 nm, must be observed to fully appreciate their distribution, such as shown in Fig. 2(b).

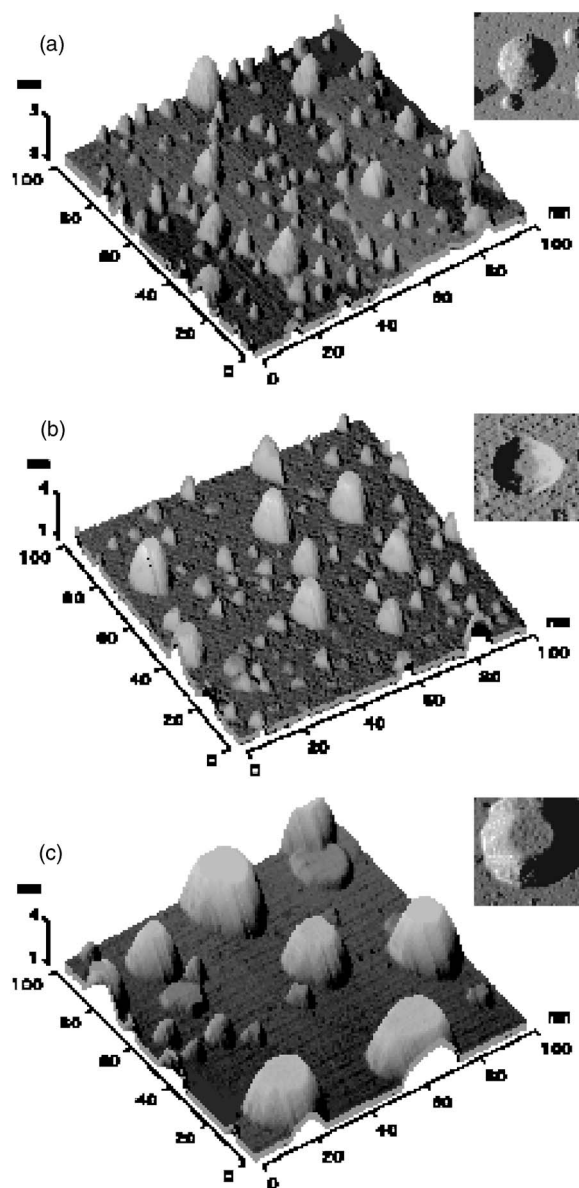


FIG. 1. 3D representation of constant-current STM images ($100\text{ nm} \times 100\text{ nm} \times 3\text{ nm}$) of titanium silicide nanocrystals after (a) $560\text{ }^\circ\text{C}$ ($100\text{ nm} \times 100\text{ nm} \times 2\text{ nm}$), (b) $600\text{ }^\circ\text{C}$ ($100\text{ nm} \times 100\text{ nm} \times 3\text{ nm}$), and (c) $660\text{ }^\circ\text{C}$ annealing temperatures ($100\text{ nm} \times 100\text{ nm} \times 3\text{ nm}$). 2D current-images of nanocrystal shapes characteristic of each temperature are shown in the respective insets.

Comparison between Figs. 2(a) and 2(b) emphasizes the differences between the “domes” and the “superdomes,” respectively.

These “superdomes” appear to be split in two, in the vertical direction, where both the upper and the lower halves seem to be terminated by a hexagonal top facet [see inset in Fig. 2(b)]. This breaking-up and flattening continue upon further annealing, as shown in Fig. 2(c). The same process is taking place in the “domes,” as shown in Figs. 2(d) and 2(e), i.e., the “domes” [Fig. 2(d)] de-bunch [Fig. 2(e)] and, eventually break-up into ill-defined stacks of multiple bunched terraces, and 2D triangular and hexagonal islands

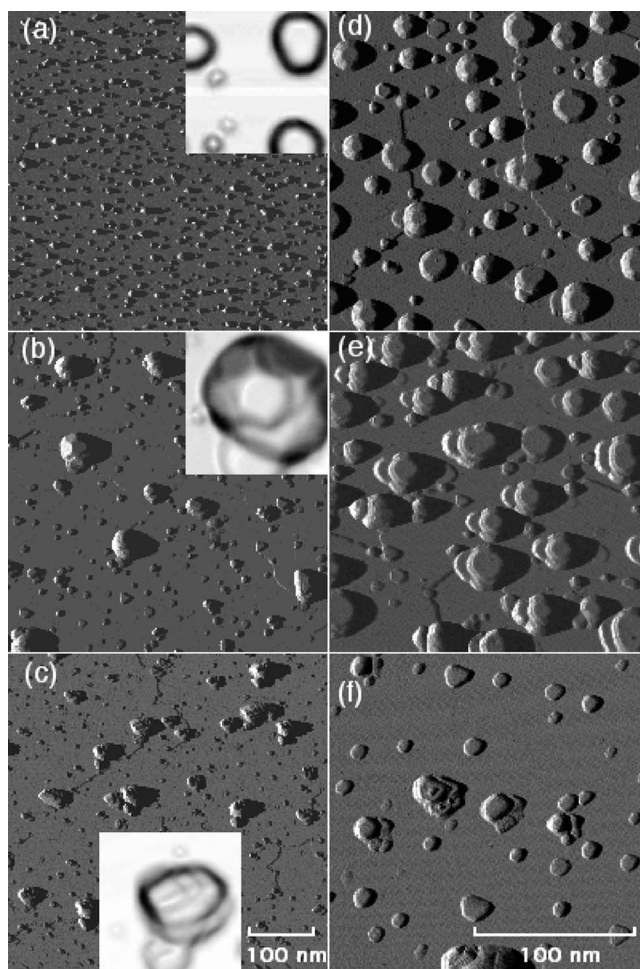


FIG. 2. (a)–(c) Large area scans showing the formation of (b) “superdomes” from (a) “domes,” with the subsequent 3D-to-2D transformation via de-bunching of the superdomes (c) and the domes (d)–(f), at several locations and magnifications during $700\text{ }^\circ\text{C}$ and $750\text{ }^\circ\text{C}$ anneals [hence the similar appearance of (c) and (f)]. Note, however, the differences between the size of the scanned areas in (a)–(c) and (d)–(f). (a) $T=700\text{ }^\circ\text{C}$, (b) $700\text{ }^\circ\text{C} < T \leq 750\text{ }^\circ\text{C}$, (c) $T=750\text{ }^\circ\text{C}$. At some other locations on the specimen’s surface mostly domes are observed, even at the (d) beginning of the $750\text{ }^\circ\text{C}$ anneal. (e) A few hours later at $750\text{ }^\circ\text{C}$, the domes undergo a massive de-bunching process, ultimately resulting in a (f) complete 3D-to-2D transformation after an overnight $750\text{ }^\circ\text{C}$ -anneal.

[Fig. 2(f)]. Closer inspection reveals that these stacked complexes form triangles and hexagons upon de-bunching, as well, as displayed in Fig. 3, so that the final surface after an overnight $750\text{ }^\circ\text{C}$ anneal consists of mostly 2D triangular and hexagonal islands. It should be noted here, that He *et al.*⁹ have shown that such flat triangular islands are, in fact, relaxed C54-TiSi_2 phase with $(01\bar{3})$ atomic plane parallel to $\text{Si}(111)$, and Ozcan *et al.*¹⁰ have found similar orientation of $\text{C54-TiSi}_2(\bar{1}0\bar{3}) \parallel \text{Si}(111)$.

IV. DISCUSSION

Such behavior is fully consistent with the generalized Wulff-Kaishew theorem, as formulated by Müller and

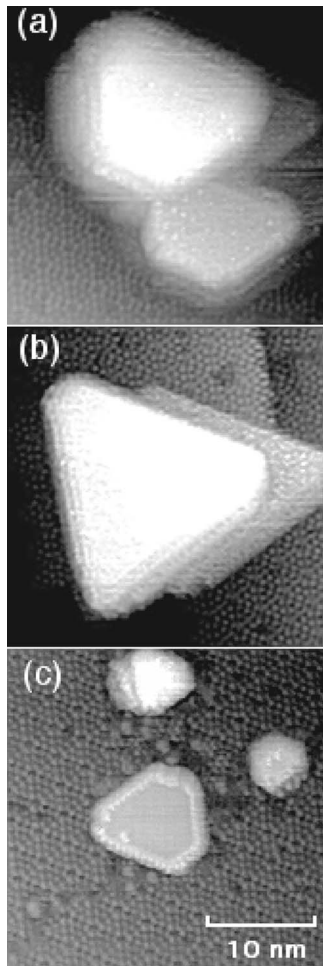


FIG. 3. High-resolution STM topographs, showing further equilibrium shape transformation of the (a) de-bunched “superdomes” and “domes,” into (b) initially triangular and eventually (c) more hexagonal 2D islands, captured at various locations on the sample’s surface following an overnight anneal at 750 °C.

Kern,^{11–13} where the equilibrium crystal shape (ECS) is obtained when all the partial derivatives of the free energy change upon the formation of 3D island on the substrate, ΔF , simultaneously vanish. In other words when $\partial\Delta F/\partial S_i|_{AB}=0$ and $\partial\Delta F/\partial S_{AB}|_i=0$ ($i \neq A, AB$), where “ i ” designates an inclined island facet of area “ S_i ,” “ A ” stands for the top facet, and “ AB ” for the interface. This leads to the set of connected equations^{11–13} for all $i \neq A, AB$:

$$\frac{\Delta\mu - B\varepsilon^2 R}{2} = \frac{\gamma_i - \gamma_A \cos \theta_i + B\varepsilon^2 \frac{V}{n_i} \frac{\partial R}{\partial S_i}}{h_i - h_A \cos \theta_i} \Big|_{AB} \quad (1)$$

$$\frac{\Delta\mu - B\varepsilon^2 R}{2} = \frac{2\gamma_A - \beta + B\varepsilon^2 V \frac{\partial R}{\partial S_{AB}}}{H} \Big|_i \quad (2)$$

In these equations “ V ” is the nanocrystal volume, “ B ” is the combination of elastic coefficients, “ ε ” is the epitaxial mismatch between the epilayer (a_A) and the substrate (a_B) lattice

constants $\varepsilon=(a_B-a_A)/a_A$, $0 < R < 1$ is the relaxation factor ($R=0$ for a completely relaxed system and $R=1$ for a nonrelaxed crystal), “ γ_i ” is the specific surface energy of the “ i ” facet, “ θ_i ” is the “ i ” facet inclination angle, “ S_i ” is the area of the “ i ” facet, “ n_i ” is the number of crystallographically equivalent “ i ” facets of area S_i , and “ h_i ” is the height normal to a facet “ i ” from the Wulff point. Finally, $H=h_A+h_{AB}$ is the total crystal height above the substrate, $h_i-h_A \cos \theta_i$ is the measure of the top face “ A ” limited by the oblique facet “ i ,” and “ β ” is the adhesion energy between the nanocrystal “ A ” and the substrate “ B .” Obviously, the number of these coupled equations equals the number of the nonequivalent facets. Clearly, the more trivial cases of freestanding or lattice-matched crystals ($\varepsilon=0$) are unsuitable for pseudomorphic heteroepitaxy. Yet, the important conclusion from analyzing these cases is that such crystals will grow in a self-similar, ECS-preserving fashion, either around the Wulff point or around some other point that coincides with the Wulff point if the adhesion energy $\beta=\gamma_A$, or shifts to above (below) the substrate surface when $0 < \beta < \gamma_A$ ($\beta > \gamma_A$). In the lattice-mismatched heteroepitaxy, the partial derivatives of the relaxation factor with respect to the facet extension will change the ECS, since for a given interfacial area each oblique facet extension helps in strain relaxation, i.e., $\partial R/\partial S_i|_{AB} < 0$, whereas the extension of the interface increases the elastic energy, $\partial R/\partial S_{AB}|_i > 0$. Thus the elastic relaxation argument favors continuous increase of the crystal vertical aspect ratio $r=H/(h_i-h_A \cos \theta_i)$ with increasing volume, rather than preserving it, as defined by the ratio of the coupled equations (1) and (2)! However, the elastic energy accumulated in the strained growing crystal, which increases with the crystal thickness (volume), may eventually cause plastic relaxation by misfit dislocations at the interface. In this case, each dislocation with an in-plane Burger’s vector component “ b ,” that enters the interface containing N interfacial dislocations, causes the misfit strain to drop to the following value:¹¹

$$\varepsilon' = \varepsilon - N \frac{b}{\sqrt{S_{AB}|N}} \quad (3)$$

Hence, once more, the ECS will adjust to the new, lower mismatch, by accordingly lowering the vertical aspect ratio and flattening the crystal. The analysis by Müller and Kern provides an excellent tool for evaluating the state of strain of the epitaxial nanocrystals, by inspecting the behavior of their vertical aspect ratios with growth. It can be formulated in the following rules:

(1) In the absence of mismatch strain, a self-similar growth, i.e., preservation of the nanocrystal shape, is expected.

(2) If the strain is present in the growing nanocrystals, it acts against wetting by thickening the crystal and thus increasing its vertical aspect ratio. This process is facilitated by the expansion of the oblique facets at the expense of the interfacial and the top facet areas. Ultimately, such process causes a complete elimination of the top crystal facet, leading to a pointy apex appearance.

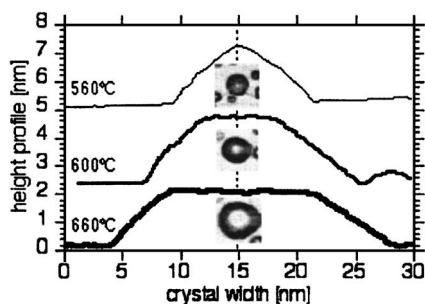


FIG. 4. Cross-sectional scan profiles describing the flattening of the silicide nanocrystals with increasing size, due to increasing temperature.

(3) When the nanocrystals grow beyond some “critical thickness,” they are no longer able to accommodate the elastic strain energy, and misfit dislocations set in, with each dislocation relaxing the strain by the amount proportional to the in-plane component of its Burger’s vector. This causes the effect opposite to the apex sharpening described above, namely the crystal flattens by developing top facet.

The titanium silicide nanocrystal islands evolution with annealing temperature, shown in Fig. 1, conforms well initially to case 2, and finally to case 3 above. Figure 4 shows the height profiles scanned across typical nanocrystals at those three temperatures, and the evolution of small pointy cone-shaped islands into flat-topped domes (with increasing island size) is apparent. It is also helpful to monitor the height and vertical aspect ratio of the evolving nanocrystals as a function of size, as shown in Fig. 5. Initially, the height increase is rather steep relative to the base widening [filled circles and broken fit in Fig. 5(a)] up to approximately the half-base width of about 9 to 10 nm, indicated by a vertical line. This range corresponds to evolution of the lens-shape silicide nanocrystals into cones¹⁴ shown in Fig. 1(a) and the upper plot-profile in Fig. 4. Upon exceeding this size, their peaks begin to flatten, as stems from Fig. 1(b) and the middle plot-profile in Fig. 4. This trend continues at a slower rate of the height increase with respect to the half-base [empty circles and dotted fit in Fig. 5(a)] with further nanocrystal flattening and top facet expansion [Fig. 1(c) and bottom plot-profile in Fig. 4].

This, again, fully agrees with the generalized Wulf-Kaishew formalism of Müller and Kern, where the height grows faster than the base for strained nanocrystals, increasing the vertical aspect ratio and leading to sharp-apex cones, whereas upon strain relaxation by misfit dislocation the opposite action takes place. *In other words, nanocrystal growth beyond the critical size introduces and increases the number of misfit dislocations, which, in turn, flatten the crystal and enlarge its top facet!* This critical value in titanium silicide nanocrystals corresponds to a lateral size of 9 to 10 nm, which is roughly about 330–350 nm³ in volume [marked by thin vertical lines in Figs. 5(a) and 5(b), respectively]. Indeed, at this volume the vertical aspect ratio drops sharply [empty squares and dotted fit in Fig. 5(b)], accompanied by simultaneous and similarly sharp widening of the top facet area [filled squares and broken fit in Fig. 5(b)]. Thus the scenario, where the titanium silicide nanocrystals remain co-

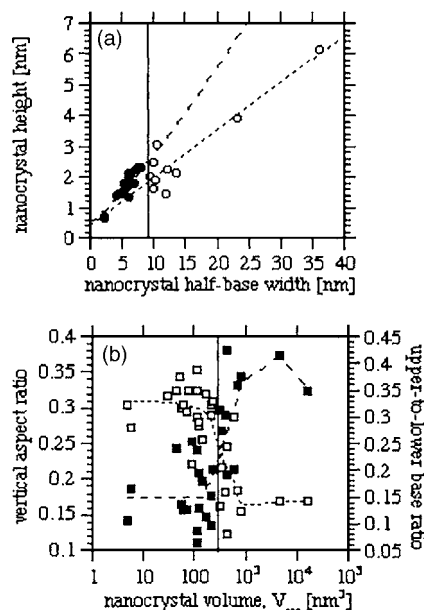


FIG. 5. Variation with size of the (a) nanocrystal height (circles), and (b) vertical aspect ratio (empty squares) and top facet-to-base ratio (filled squares). In (a), filled circles designate “drop-lets” (or “lenses”) and “cones,” whereas empty circles represent “domes” and superdomes. Vertical lines in (a) and (b) mark the critical size for “cone-to-dome” transition, and dotted and broken lines are for eye guidance only.

herent with the substrate until they reach the critical lateral dimension of about 9 to 10 nm (330–350 nm³ volume), at which point misfit dislocations set-in and relax the strain, causing nanocrystal flattening, seems reasonable in view of the experimental findings presented here. In this particular case of Ti/Si(111), shape transformation is further complicated by phase transformation. It is well known that epitaxy of C49-TiSi₂ on Si(111) is even more difficult than that of C54-TiSi₂, since the latter, in spite of the large nominal mismatch, can form several epitaxial orientation relations with Si(111) surface that minimize the mismatch, at least, along certain crystallographic directions.¹⁰ Hence, it is reasonable to assume, that the annealing not only causes the silicide nanocrystals to grow, but also leads to the C49 formation and subsequent C49-to-C54 phase transformation, providing in the process an additional (to the Wulf-Kaishew) activation for dislocation nucleation.

The flattening, ultimately transforming 3D “domes” and “superdomes” into flat 2D islands, requires massive atomic rearrangement, mass transport, and surpassing activation barriers. In a roughly round-shape crystallite, truncated by certain faces, face advancement requires mass transfer from the curved regions onto a flat face, while face retreat requires mass transfer in the opposite direction. Generally speaking, creation of a circular island of radius “*r*” and height “*h*” on a face of radius “*ρ*” intersecting the curved portion of a truncated sphere (with “*R*” radius of curvature) at an angle “*θ*”, can be achieved either by nucleating a disk of volume $\pi r^2 h$, or by removing a ring of volume $\pi(\rho^2 - r^2)h$. Since $\rho = R \sin \theta$, and assuming the island edge formation energy, γ_{step} , is related to the free energy of the curved portion of the

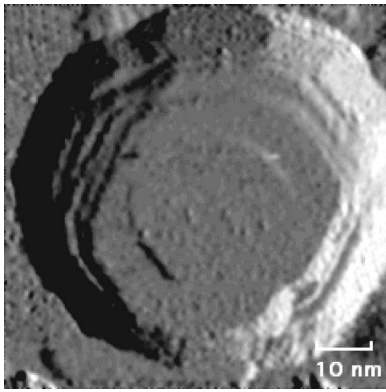


FIG. 6. Screw dislocation emerging at the top facet of a “superdome.”

crystal, γ_{curve} , as $\gamma_{\text{step}} = \gamma_{\text{curve}} \sin \theta$, the barrier, which, in general, can be symmetric with respect to the addition or removal, depends linearly on the face and crystal size, as:¹⁵

$$E_b = \frac{1}{2} \pi h R \frac{\gamma_{\text{step}}^2}{\gamma_{\text{curve}}} = \frac{1}{2} \pi h R \frac{(\gamma_{\text{curve}} \sin^2 \theta)}{\gamma_{\text{curve}}} = \frac{1}{2} \pi h R \gamma_{\text{curve}} \sin^2 \theta$$

$$= \frac{1}{2} \pi h \rho \gamma_{\text{curve}} \sin \theta \quad (4)$$

Even in the most favorable case, where material must be transferred from the face to the curved portion of the crystal to reach the ECS from a nonequilibrium state (such as in this work), with asymmetric barrier smaller than that for mass transfer in the opposite direction, the faces can enlarge only to about 0.50–0.75 of their equilibrium size.¹⁶ Beyond this, the barrier becomes prohibitive for crystals larger than a few nanometers,^{15–17} unless step-forming defects, such as screw dislocations, emerge. In view of the large “superdome” (or even “dome”) sizes, their flattening and de-bunching would not have been possible without the aid of screw dislocations. Indeed, screw dislocations were frequently found to emerge at the “dome” and “superdome” tops, as shown in Fig. 6. It thus could be concluded, that “superdomes” are, in fact, very large “domes” containing screw dislocations, in addition to misfit dislocations.

Flattening and development of flat tops, i.e., 3D-to-2D transition, is not the only process observed to take place. The equilibration continues in the 2D state, as well: The debunching of the “domes” and “superdomes” results in the initially triangular islands, which gradually transform into a more hexagonal shape by annihilating the sharp triangular corners. This process is quite similar to the reported by Voigtländer for the Si(111) islands.¹⁸ During the de-bunching, significant mass transport takes place, which locally reproduces the state of growth in the vicinity of the nanocrystal, although no material flux is coming from the evaporator. During growth, the first species are added to the fast-growing edges perpendicular to substrate’s Si[11 $\bar{2}$] and Si[$\bar{2}$ 11] directions, so that roughly hexagonal tops of the de-bunching complexes become triangular for the time of de-bunching and rearrangement. (According to the analysis of He and co-workers⁹ the edges of the relaxed triangular C54-TiSi₂ (01 $\bar{3}$) island’s are

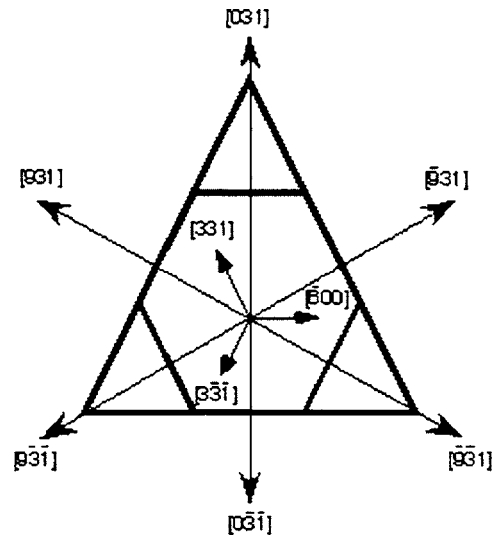


FIG. 7. Geometry of relaxed triangular titanium silicide island, with respect to relevant crystallographic directions.

parallel to its [331], [3 $\bar{3}$ 1], and [$\bar{4}$ 00] directions, which means their motion directions are [$\bar{9}$ 31] and [031] or [$\bar{9}$ 31] and [931], cf. Fig. 7). Then, when left to equilibrate in the already 2D state, reduced “vapor pressure” or adatom concentration around the islands causes Gibbs-Thomson effect of island dissolution, with the triangle corners first to retreat, due to their lower (relative to the triangle edges) coordination. Finally, it follows from the inspection of Fig. 3 that the in-plane orientation of the triangular and hexagonal silicide islands is such that their edges are parallel to Si<110> directions, i.e., during growth (shrinkage) their outward (inward) motion is along Si<112> directions. One possible explanation for such an orientation is an anisotropic lattice mismatch between the C54-TiSi₂ (013) and Si(111) atomic planes, with about 5% along Si<112> directions and twice as much (~10%) along Si<110> directions!¹⁰

V. CONCLUSIONS

In summary, vast majority of titanium silicide nanocrystals deposited at RT and subsequently annealed at lower than 600 °C temperatures are coherent with Si(111) substrate and assume mostly conical shape. Small fraction of the silicide material populates two-dimensional triangular and hexagonal islands. These flat islands are believed to consist of the equilibrium terminal C54-TiSi₂ phase that, possibly, formed at such an unusually low temperature (<600 °C) due to some local kinetics. Their orientation relations with the Si(111) surface reflect minimization of mismatch-induced epitaxial strain. The majority, however, keeps growing with temperature in a 3D fashion, with the size increase followed by a strong reduction of the island number density (indicating an Ostwald ripening type mechanism¹⁴). Above 600 °C, island growth was accompanied by a progressive truncation of the cones and flattening, resulting in the island shape transformation of cones into multifaceted domes and superdomes. Such behavior was consistent with strain reduction due to the

introduction of misfit dislocations at the growing interface, in accord with Wulf-Kaisew theorem of equilibrium crystal shapes, as well as with the expected C49- and C54-TiSi₂ phase formation and transformation kinetics. Aided by step-forming screw dislocations at a 700 °C–750 °C range, the domes and the superdomes de-bunched to keep flattening

and forming 2D hexagonal islands, which are believed to be the stable equilibrium shape of C54-TiSi₂ nanocrystals. During rearrangement of the de-bunching material, C54-TiSi₂ nanoislands attain intermediate triangular growth shape, but upon growth interruption hexagonal shape is restored.

*Corresponding author. Email: ilang@eng.tau.ac.il

¹S. P. Murarka, *Silicides for VLSI Applications* (Academic Press, New York, 1983).

²R. Beyers and R. Sinclair, *J. Appl. Phys.* **57**, 5240 (1985).

³A. W. Stephenson and M. E. Welland, *J. Appl. Phys.* **78**, 5143 (1995).

⁴A. W. Stephenson and M. E. Welland, *J. Appl. Phys.* **77**, 563 (1995).

⁵G. Medeiros-Ribeiro, D. A. A. Ohlberg, D. R. Bowler, R. E. Tanner, G. A. D. Briggs, and R. S. Williams, *Surf. Sci.* **431**, 116 (1999).

⁶G. A. D. Briggs, D. P. Basile, G. Medeiros-Ribeiro, T. I. Kamins, D. A. A. Ohlberg, and R. S. Williams, *Surf. Sci.* **457**, 147 (2000).

⁷I. Goldfarb and G. A. D. Briggs, *Phys. Rev. B* **60**, 4800 (1999).

⁸J. Oh, V. Meunier, H. Ham, and R. J. Nemanich, *J. Appl. Phys.*

92, 3332 (2002).

⁹Z. He, M. Stevens, D. J. Smith, and P. A. Bennett, *Surf. Sci.* **524**, 148 (2003).

¹⁰A. S. Özcan, K. F. Ludwig, Jr., P. Rebbi, C. Lavoie, C. Cabral, Jr., and J. M. E. Harper, *J. Appl. Phys.* **92**, 5011 (2002).

¹¹P. Müller and R. Kern, *Surf. Sci.* **457**, 229 (2000).

¹²P. Müller and R. Kern, *Appl. Surf. Sci.* **162-163**, 133 (2000).

¹³P. Müller and R. Kern, *Appl. Surf. Sci.* **164**, 68 (2000).

¹⁴I. Goldfarb, S. Grossman, G. Cohen-Taguri, and M. Levinshtein, *Appl. Surf. Sci.* **238**, 29 (2004).

¹⁵W. W. Mullins and G. S. Rohrer, *J. Am. Ceram. Soc.* **83**, 214 (2000).

¹⁶C. L. Rohrer, G. S. Rohrer, and W. W. Mullins, *J. Am. Ceram. Soc.* **84**, 2099 (2001).

¹⁷H. P. Bonzel, *Phys. Rep.* **385**, 1 (2003).

¹⁸B. Vöggtlander, *Surf. Sci. Rep.* **43**, 127 (2001).